RIPPLED DEPOSITS: FORMATION AND PRESSURE DROP EFFECTS

J.S. Gudmundsson[+]
I.H. Newson[*]
T.R. Bott[+]

ABSTRACT

The literature relating to the incidence of naturally occurring rippled deposits in process plant and super-critical once-through boilers has been surveyed. Characteristics of rippled surface geometry and the mechanism of formation are identified and discussed. The excessive pressure drop penalty associated with rippled surfaces in comparison with sand-grain-type roughness is shown in terms of boundary layer theory. The pressure drop characteristics of other artificially formed roughnesses, e.g., repeated rib and screw-thread types, are also discussed.

A variety of simulated rippled surfaces were formed on 25 mm OD brass tubing by impressing circular indentations of varying depth at different spacings. Pressure drop measurements were obtained for single phase fluid (water) flow in eighteen such tubes over a Reynolds Number range 10^4 to 3.10^5. Pressure drop measurements were also taken with air flow in a 12.5 mm OD brass tube having a naturally formed rippled silica deposit on its inner surface. These results were analysed with a view to providing a means of predicting pressure drop in a rippled surface geometry.

+ University of Birmingham
* Chemical Engineering Division

Heat Transfer and Fluid Flow Service,
AERE, Harwell.
and National Engineering Laboratory

March, 1977

HL77/572
/KE

CONTENTS

TABLES

ILLUSTRATIONS

CONTENTS (Continued)

1. Introduction

The formation of deposits on pipe and channel surfaces may result in changes in their heat transfer[1] and pressure drop characteristics. Deposition will decrease the pipe diameter and usually increase the surface roughness. These effects will increase the pressure drop and improve the heat transfer performance. The thermal resistance of the deposit, however, will decrease the overall heat transfer coefficient.

The extent to which deposition will affect heat transfer and pressure drop will depend on the type of roughness being formed. Under certain conditions it is possible for a transversely rippled deposit to be formed which exhibits a more pronounced effect on the flow conditions at the wall than any other natural roughness shape. Such deposits have been observed in some process equipment and similar effects can be recognised in sandy deserts and beaches. A study of rippled surfaces, their formation and pressure drop effects, is important so that proper design and efficient operation of process plant may be achieved.

2. Examples of Rippled Surfaces

Rippled surfaces have been observed in a number of different situations.

2.1 Rippled Surfaces in Pipelines Carrying Fresh Water

Wiederhold[2] and Seiferth & Kruger[3] reported that excessive pressure loss increase occurred in a pipeline carrying fresh water. In three years the pressure drop increased by about 57%. The pipeline was 80 km long with a diameter 0.5 m.

The pressure drop increase was due to the formation of transversely rippled deposits. The ripples were 0.5–1 mm high and spaced at 3–8 mm. The average ripple height (e) was 0.7 mm. The average thickness of the deposits was of the order of 2 mm, i.e., the effective diameter of the pipeline was 0.496 m[3]. The deposits consisted mainly of Al_2O_3 (52.8%), MnO_2 (19.2%), CaO (9.9%) and Fe_2O_3 (3.1%)[2].

Pressure drop measurements were performed on a 178 m section of the pipeline after 3 years of operation[2,3]. The friction factor $f(= \tau_o/\rho\bar{u}^2)$ calculated from these measurements decreased with Reynolds number as shown in Table 1.

TABLE 1

Friction Factors Obtained in a Pipeline Carrying Fresh Water[2,3]

Reynolds Number Re	Friction Factor f	
138,000	0.00705	Measured
138,950	0.00703	Estimated
316,228	0.00540	Estimated
492,000	0.00515	Measured
562,341	0.00498	Estimated

Gessner[4] reports observations on increased pressure loss in a large diameter water duct associated with a small hydroelectric scheme. The increased pressure drop was due to the formation of rippled deposits. In eighteen years the output of the plant decreased substantially from 10.1 MW to 8.6 MW or about 1% per year. The average diameter of the pipe was 1.95 m.

The thickness of the deposit after eighteen years was 1.5–12 mm. The height of the ripples (e) was 0.5–4 mm and their spacing (x) 4–16 mm. The reported ripple ratio (λ) was in the range 4–10 but if the average values of x and e are used λ becomes 4.44.

2.2 Magnetite Deposits in Boiler Systems

Experience with some supercritical once-through boilers has shown that unacceptably high pressure drops can occur in the evaporators such that frequent chemical cleaning is required. Examination of tubes removed from these boilers has shown that transversely rippled corrosion products on the walls are responsible for the high level of pressure drop encountered. The phenomenon of rippled deposits has only been observed in those sections of evaporator tubes carrying water in the liquid phase. In other sections, such as economiser tubes and steam tubes, all corrosion products are evenly distributed as thin films with no evidence of ripples.

Corrosion product films in supercritical once-through boilers are in two layers. The inner layer corresponds to the thickness of the corroded tube material; it is dense and protects the tube material from further rapid corrosion. In evaporator tubes carrying water the outer layer of deposit is more porous and is rippled[5–17]. The inner layer thickness lies in the range 5–15 μm[10–13]. The magnetite crystals of this inner layer are 0.1–0.2 μm[9,10] with pore sizes of less than 0.01 μm[10]. On the other hand, the crystals in the outer layer where the surface is rippled consist of coarse single crystals some of which are considerably rounded.

Haller et al[13,14] observed that the structure of the corrosion product film was transversely rippled. Other workers[7,8,10], however, stated that the structure ranged from a transverse ripple effect to a "crater-like" form where the transverse ripples were connected by longitudinal ripples. Schuster[9] concluded that the "crater-like" structure was more likely to be associated with high Reynolds numbers.

The average spacing (x) between the ripples has been reported as 200–350 μm[8] and 180–300 μm[10] with ripple heights (e) of 25–40 μm and 20–40 μm respectively. Some further data are given in Table 2 for different tube diameters.

TABLE 2

Ripple Ratio at Different Tube Diameters

x μm	e μm	λ	Tube Diameter d mm	Ref.
450	90	5	148	8
350	45	7.8	38	16
201	16.5	12.2	16.8	14
193	14.2	13.6	15.7	14

2.3 Rippled Deposits in a Pipeline Carrying Saturated Brine

Rippled deposits have been observed in a 0.61 m pipeline conveying saturated brine at 15°C[18]. Exceptionally high pressure drop resulted which could not be explained simply in terms of increased velocity due to the reduction in flow area. The thickness of the deposit was 5-7 mm with 6 mm considered as the average, i.e., the effective diameter of the pipe was therefore approximately 0.589 m. The deposits consisted mainly of $CaCO_3$ and $Mg(OH)_2$.

Measurements on a 2692 m section of the pipeline after approximately 5 years of operation showed that the pressure drop was 0.365 bar at a Reynolds number (Re) of 139,000 (bulk velocity 0.5 m/s). The measured friction factor was 0.00738. A section of the deposit with four transverse ripples (see Figures 1 and 2) was measured giving an average ripple spacing (x) of 4.73 mm and an average ripple height (e) of 1.08 mm. The pressure drop calculated from sand grain roughness theory[21] using the average ripple height is only 0.140 bar, or 38% of the measured pressure drop.

2.4 Rippled Deposit from Geothermal Water

In studies of deposition (59.4% silica) from geothermal waters in heat exchanger tubes[19] rippled surface have been observed. The geothermal water entering a heat exchanger was about 80°C and saturated with silica. The average Reynolds number was 44000 based on the clean tube ID of 10.3 mm. When the tube was removed after 2000 hours of operation the volumetric diameter was measured as 9.55 mm.

A section of the silica deposit was removed to measure the dimensions of the ripples (see Figures 1 and 2). This was done by taking a photograph of a polished cross section of the deposit and then magnifying at 50x. The height and spacing of 38 ripples were measured. The average spacing (x) was found to be 0.87 mm and the average ripple height (e) = 0.123 mm. The standard deviation of 38 spacing and height measurements was, respectively, 36.5% and 33.1%. This is about the same as a normal distribution that is characteristic of many naturally occurring phenomena.

3. Pressure Drop in Rough Pipes

The usual equation used for estimating pressure drop in pipes and channels is of the form[20]

$$\Delta p = 8f \frac{l}{d} \frac{\rho \bar{u}^2}{2} \qquad (1)$$

where Δp is the pressure drop, f is the friction factor, l and d are the length and diameter of the pipe, ρ is the fluid density and $\bar{u}$ the bulk velocity. The friction factor f ($= \tau_o/\rho\bar{u}^2$) used throughout this present work is that of Coulson and Richardson[20] and equals ½ the Fanning friction factor, and ⅛ the dimensionless "Coefficient of Resistance" used by Schlighting[21]. The characteristics of a surface as they affect pressure drop are included in the value of the friction factor.

The friction factor in rough pipes can be related to the friction function Φ by the expression[21,22,24]

$$\Phi = \sqrt{\frac{1}{f}} + 2.5 \ln\left(\frac{e}{R}\right) + 3.75 \qquad (2)$$

where e is the roughness height and R the pipe radius. The friction function depends on the geometry of a rough surface[22].

3.1 Sand Grain Roughness

Nikuradse[23] studied the pressure drop in pipes having a variety of sand grain roughnesses. For this surface geometry he was able to correlate the friction function to the dimensionless roughness height $e^+ = u^* e/\upsilon$, where u^* is the friction velocity $\left(= \left(\frac{\tau_o}{\rho}\right)^{\frac{1}{2}}\right)$ and υ the kinematic viscosity. The roughness height was taken as the diameter of the sand grains. The values of friction function Φ, and e^+, as determined by Nikuradse[23] for all the sand grain surfaces when plotted generated the single curve shown on Figure 3.

Nikuradse[23] identified three regions of flow[21]. These are:

$e^+ \leqslant 5$	hydraulically smooth region,
$5 \leqslant e^+ \leqslant 70$	transition region,
$e^+ > 70$	completely rough region.

In the smooth and transition regions Φ varied with e^+. In the rough region, however, the friction function was constant at $\Phi = 8.5$ such that the friction factor calculated from Eq. (2) was independent of Reynolds number.

3.2 Rectangular Roughness

Considerable work has been done on surfaces with transverse, rectangular rib roughness. Recently a relationship for the friction function Φ for this type of surface has been established by Baumann and Rehme[22]. They based their evaluation on the experimental data presented in the literature by 35 authors. Since the friction function Φ for rectangular roughness shapes becomes constant in the completely rough region, as for sand grain roughness, only data for $e^+ \geqslant 100$ was used in their analysis.

Baumann and Rehme derived an empirical expression for Φ in terms of the geometrical parameters x/e, e/w and e/r. The geometry of rectangular roughnesses is shown in Figure 4 where x is the pitch, e the height and w the width of the rectangular rib. The parameter r is the length of the velocity profile between the wall and the zero shear position. In circular tubes this corresponds to the radius. In all their work Baumann and Rehme[22] used the volumetric diameter.

The friction function derived by Baumann and Rehme[22] was

$$\Phi = 0.345\, \Phi_\alpha \Phi_\beta \qquad (3)$$

where α refers to an expression giving the dependence on x/e and e/w; while β refers to an expression giving the dependence on e/r. The α-expression was

$$\Phi_\alpha = a_1 \left(\frac{x}{e}\right)^{a_2} + a_3 \left(\frac{x}{e}\right)^{a_4} \qquad (4)$$

with

$$a_1 = 18.5 \left(\frac{e}{w}\right)^{-0.9475}$$

$$a_2 = -1.143 \left(\frac{e}{w}\right)^{-0.147}$$

$$a_3 = 0.33 \left(\frac{e}{w}\right)^{0.1483}$$

$$a_4 = 0.758 \left(\frac{e}{w}\right)^{-0.11}$$

The expression is valid when

$$1 \leqslant \frac{x}{e} \leqslant 40$$

$$0.3 \leqslant \frac{e}{w} \leqslant 8$$

$$\Phi_\alpha \leqslant 10$$

and gives a maximum deviation of 8% from the experimental data. The β expression was a polynomial of the form

$$\Phi_\beta = 2.9 + 1.49 \left(\frac{e}{r}\right) - 1.972 \left(\frac{e}{r}\right)^2 \qquad (5)$$

It should be noted that when $e/r \to 0$ the β-expression becomes $\Phi_\beta \sim 2.9$ such that in Eq. (3) $\Phi \sim \Phi_\alpha$. In the present work the limited influence of e/r on Φ will be neglected. For the e/w values of 0.5 and 1.5 the friction function Φ was calculated and is shown in Fig. 5.

3.3 Other Types of Roughness

Streeter[25] has studied the pressure drop in 50 mm diameter pipes in which screw threads of a very close pitch had been cut in the inner surface. By varying the profile of the cutting head he was able to produce several different shapes of inner roughness. The three roughness shapes considered here are shown in Figure 6, where the length scales and the ratio of pitch to height are also given. From the data presented by Streeter[25] the friction function Φ has been calculated here and plotted in Figure 7. On Figure 7 the dotted line is that presented by Nikuradse[21,23] for sand grain roughness. No general relationships were presented by Streeter[25] for the roughness types investigated.

Haller et al[13,14] measured the friction factor in several tubes with in-service-generated magnetite deposits. They found that, as with sand grain and rectangular rib roughness, the friction function Φ became independent of e^+, the dimensionless roughness height. In the completely rough region Φ is approximately equal to 5.

Using this value in Eq. (2), Haller et al[13,14] found that the calculated friction factor had an average deviation of 6% and a maximum deviation of 10% from measured values. The ripple ratio for the tubes tested by Haller et al[13,14] was probably in the range 12-14.

4. Pressure Drop Experiments

4.1 Rippled Surfaces of Geothermal Silica

Pressure drop measurements were performed on a 12.5 mm OD heat exchanger tube that had a rippled silica deposit (see Section 2.4 above). A photograph of a section of the tube is shown in Figure 1 and a typical profile of the ripples is shown in Figure 2. The pressure drop measurements were performed on a 38 cm long section of this tube. The ID of the clean tube was 1.026 cm but the diameter of the tube within the deposit was estimated volumetrically as 0.955 cm.

The experimental set-up consisted of a 90 cm long, 1.026 cm ID, entry section connected to the test section. The ID of both tubes was flush to a 6.4 mm bridge between them having two radially-opposite pressure tappings in the middle. Similarly, there was a 40 mm long tube downstream from the test section. Since the ID of the clean test section was flush with the inlet and outlet tubes there existed a small step in the transition from smooth to rippled surfaces.

Compressed air was used in the experiments. The flowrate was measured by a gas meter downstream at atmospheric pressure. The temperature of the air was measured between the 40 cm outlet section and the gas meter. The pressure tappings at the inlet and outlet were connected to a water manometer with the other leg open to atmosphere. In this way the average absolute pressure and pressure drop in the test section could be determined.

To test the validity of the experimental procedure a smooth test section was inserted and the pressure drop characteristics were determined. The friction factor values derived from the measured pressure drop were found to fall just above those of a hydrodynamically smooth tube, when plotted against Reynolds number. This is to be expected for a commercially rough tube.

The friction factor against Reynolds number plot for the rippled tube is shown in Figure 8. The friction factor increases with Reynolds number to an apparently constant value. This is in qualitative agreement with tubes having sand grain roughnesses[21,23]. However, the friction factor is much higher than predicted from sand grain roughness theory using the ripple height as the characteristic dimension. The average ripple height was measured as 0.123 mm. Assuming fully turbulent flow, sand grain roughness theory predicts a friction factor of 0.0052, while the experimental value is approximately 0.014, or 170% higher. To compare the experimental results with the semi-empirical sand grain roughness theory the friction function Φ has been calculated and is shown plotted in Figure 9 against the dimensionless roughness height e^+. In the fully rough region, where Φ is independent of e^+, the value of the friction function becomes $\Phi \simeq 3$.

4.2 Pressure Drop Measurements on Simulated Ripple Surfaces

Simulated ripple surfaces were manufactured by impressing circular indentations at given separation distances x along the length of a number of 25 mm OD brass tubes. By varying the depth of indentation e at four different values of the spacing x it was hoped that a range of values $\lambda = x/e$ could be obtained. The manufacturing method, however, encountered problems of tube deformation when attempting to produce indentations, i.e., roughness heights within the tube, larger than about 0.25 mm. In the event therefore the complete range of desired x/e values was not achieved. Table 3 below gives the actual dimensions achieved in the 18 tubes tested so far. The programme of tests is not complete and further experiments will be conducted with tubes having larger roughness heights when these become available.

TABLE 3

Dimensions of Tubes with Simulated Ripple Surfaces
(all tubes initially 25 mm OD × 0.7 mm wall thickness)

Tube Number	Spacing between indentations x	Depth of indentations e	"Ripple" Ratio $\lambda = x/e$
	mm	mm	
1	2.5	0.029	85.6
2	2.5	0.102	24.6
3	2.5	0.165	15.1
17	2.5	0.279	8.95
18	2.5	0.394	6.35
5	5.1	0.0165	309
6	5.1	0.0635	80.3
7	5.1	0.114	44.6
8	5.1	0.191	26.8
9	8.89	0.013	700
10	8.9	0.038	233
11	8.9	0.165	53.8
12	8.9	0.203	43.7
13	12.7	0.051	250
14	12.7	0.038	333
15	12.7	0.203	62.5
16	12.7	0.229	55.6
26	12.7	0.432	29.4

The roughness heights within the tube were measured by making a wax impression of short lengths of the inner tube surface. The resulting wax casting also showed the shape of the roughnesses, and the internal profile. Figure 10 shows tracings of several such profiles. The length of tube which was profiled was 114 cm in each

case. For purposes of calculation the true average cross-sectional area of flow in each tube was obtained by filling the tube with a measured volume of water over a known length. The average internal diameter was then computed from this area by assuming a circular tube.

4.2.1 Experimental Programme and Results

Each of the indented tubes was tested by taking pressure drop measurements over a range of water flow rates within the tube. Experiments were conducted with cold water flow at about $20^{o}C$ and hot water flow at about $90^{o}C$. The Reynolds number range covered by this means extended from about 10^{4} to 3.10^{5}.

The experimental readings were converted to plots of the Moody friction factor f ($= \tau_o/\rho\bar{u}^2$) against Re No. Values of the function Φ were also computed from Eq. (2). Figure 11 shows, as an example, plots of f vs Re No for a series of tubes where the spacing of the indentations is constant at 2.5 mm, while the roughness height increases from 0.10 to 0.39 mm. For the three larger roughness heights the flow is clearly in the fully turbulent region, i.e., where f is independent of Re No, over the upper half of the Reynolds number range.

Figure 12 shows the computed values of the function Φ plotted against e^+ for each of these four tubes. Also shown on this figure is the unique curve which applies for all sand grain heights on sand grain type surfaces. There is clearly no single curve for all roughness heights of these simulated ripple surfaces even though the data plotted on Figure 12 refers to identical ripple spacing x. Only the two tubes with the largest simulated ripple heights have reached the completely rough regime as shown by the near constant value of Φ. It is in fact in this fully rough regime in which analysis is easiest and the plots show that the experiments need to be extended to much higher Re No values to reach the fully rough regime for those tubes with the smaller simulated ripple heights. Or, alternatively, tubes with larger similated ripple heights should be studied. This second course is the one being pursued and is dependent upon satisfactory manufacturing methods being developed to produce the larger ripple heights, say 0.5 mm and larger. Of all the tubes with simulated ripple surfaces listed in Table 3, only tubes 17 and 18 showed evidence of reaching the fully rough regime on the Φ vs e^+ plot.

5. Discussion

The review of the literature on rippled deposits shows that some information on pressure drop effects is available while the mechanism of formation remains unclear.

5.1 Formation of Ripples

The available data on the length scales of rippled deposits are given in Table 4. An examination of these data shows that the spacing x and height e of naturally-occurring ripples range from 0.193 to 10 mm and 0.0142 to 2.3 mm, respectively. The ripple ratio $\lambda = x/e$, however, ranges from 4.3 to 13.6. The ripple ratio is therefore confined to a relatively narrow range while the spacing and height show a greater

range of values. This suggests that naturally-occurring rippled deposits might be characterised by the ripple ratio rather than the actual length scales.

TABLE 4

Length Scales and Ripple Ratios of Rippled Deposits

Types of Fluid	x (mm)	e (mm)	$\lambda = \frac{x}{e}$	Reference
Fresh water	5.5	0.75	7.3	2
" "	10	2.3	4.3	4
Boiler water	0.45	0.09	5	8
" "	0.24	0.03	8	10
" "	0.35	0.045	7.8	16
" "	0.8	0.1	8	16
" "	0.193	0.0142	13.6	14
" "	0.201	0.0165	12.2	14
Saline water	4.73	1.08	4.4	Present work
Geothermal water	0.87	0.123	7.1	Present work

Webb et al[24] have presented a catalogue of flow patterns downstream from a rectangular rib roughness for several pitch to height ratios. They show that separation occurs at the rib, forming a widening free shear layer which reattaches 6-8 rib heights downstream from the separation point. A reverse flow boundary layer originates at the reattachment point and grows in thickness in the upstream direction. Webb et al[24] stated that reattachment does not occur for a pitch to height ratio $x/e < 8$. Measurements have shown that the local heat transfer coefficient reaches a maximum in the vicinity of the reattachment point.

Wilkie[29] has shown that reattachment occurs probably at $x/e = 7.2$, which is the ratio selected as most favourable for gas-cooled fuel elements[28]. Davies[26] and Davies and Shawki[27] have reached similar conclusions. Using data obtained by Abbot and Kline[30], it was estimated by Lewis[31] that reattachment occurs at $x/e = 7.5$. It is therefore evident that the transfer of heat, mass and momentum at surfaces with repeated rectangular rib roughness is greatest when the pitch or spacing corresponds to the distance at which reattachment occurs naturally behind a roughness element.

The material which is eventually deposited may originate from either the dissolved or particulate states. For material to deposit there must be some driving force such as concentration difference. One common characteristic of the systems where rippled surfaces have formed is that the deposition driving force is almost non-existent. This could be a major factor causing deposition to assume a rippled profile. When the driving force is large deposition will occur on sites evenly distributed over the surface. However, when the driving force is limited, deposition will occur preferentially at sites in regions of enhanced mass transfer.

In commercial tubes naturally-occurring roughnesses exist as a result of the manufacturing process. Such roughnesses will project into the fluid and promote deposition at the tip. At these locations the deposits will most likely grow faster than in the areas around them. But at a certain distance downstream from the roughness the deposition rate will also be enhanced due to the phenomena of boundary layer separation and reattachment. In these regions of enhanced mass transfer a new roughness element will grow and in turn give rise to further enhancement sites further downstream. In this way the mechanism of formation becomes self-perpetuating.

Rippled deposits have been shown to form under both isothermal[2,3,4,18] and heat transfer[5-17,19] conditions and circumferential heat flux appears to have no effect on the structure of the ripples[8,10,13]. This suggests that the mechanism giving rise to rippled deposits is a hydrodynamic phenomenon of the type discussed above. Ripples will presumably only be formed where the system is at, or close to, saturation, and where the material depositing adheres strongly to the surface.

The mechanisms of formation postulated by other authors suggest that the phenomenon of rippled deposits might be caused by an interaction of deposition and erosion[7,8,10] as a result of high frequency pressure/temperature/flow oscillations[16] or by the action of sublayer bursts in the boundary layer[33].

From the limited data available[30] reattachment behind roughness elements (backward-facing steps in flow channels) appears to be independent of Reynolds number. In most references[24,26,28,29] no mention is made of a dependence on Reynolds number. It has been observed by Schoch et al[8] that the ripple ratio of magnetite deposits in boilers decreased with increasing tube diameter when the fluid velocity or mass flux was kept constant. The data in Table 2 are for ripple ratios in several supercritical once-through boilers at similar mass flux conditions. The data points from references 8 and 16 are probably for identical mass flux values. The values in Table 2 have been plotted in Figure 13 and are seen to fall on a smooth curve. Since the mass flux and fluid properties are similar, the ripple ratio must be decreasing with increasing Reynolds number.

5.2 Pressure Drop Effects in Tubes with Natural Ripple Roughness

The main effect of rippled deposits is the increase in pressure drop. The friction factors in Table 1 for a pipeline carrying fresh water were plotted (data points shown as circles) in Figure 14. The friction factor decreases with Reynolds number[2,3]. Richter et al[10] reported that for all boiler tubes with rippled deposits the friction factor was 0.00313 at Reynolds number 1.6×10^6. This value (triangular symbol) and the value given in Section 2.3 for a pipeline carrying saturated brine (square symbol) have also been plotted on Figure 13. The ripple ratios for the surfaces are given in Table 4. Although the operating conditions for these three pipes are quite different, the friction factors all fall on the same straight line. The straight line can be represented by the empirical Blasius-type equation

$$f = \frac{0.25}{Re^{0.3}} \qquad (6)$$

This equation represents the data with an average deviation of approximately 5%, while the maximum deviation was just under 10%. It appears therefore, from Figure 14, that the friction factor decreases with increasing Reynolds number for flow in pipelines with rippled surfaces for several different systems.

The friction factor characteristics in Figure 14 are different from surfaces with sand grain[21,23] and rectangular[22,24,29] roughnesses. In the completely rough regime the friction factor for sand grain and rectangular roughness surfaces is independent of Reynolds number. It is unclear why the friction factor for naturally-occurring rippled surfaces should decrease with increasing Reynolds number. Schlicting[32] has, however, demonstrated that simulated ripple surfaces (right angles on a flat surface) also show this characteristic of decreasing friction factor with increasing Reynolds number provided the ripple ratio $\lambda = x/e$ is less than some critical value. His experiments indicated that this value was probably just less than 6[2,3,32].

The friction factor characteristics of the tube having a rippled silica deposit are shown in Figure 8. The friction factor is much greater than would be expected from sand grain roughness theory. This increase is comparable with the increases shown by the other naturally-occurring ripple surfaces on Figure 14.

However, the friction factor initially increases with Reynolds number in the manner characteristic of sand grain or rectangular roughnesses. Haller et al[13,14] indicated similar behaviour for rippled magnetite deposits found in boilers. This raises the question of whether deposits formed under isothermal and heat transfer conditions have different pressure drop characteristics. Gessner[4] performed pressure drop measurements on surfaces having simulated ripples. The data could not be reduced to a single empirical curve, as that for sand grain roughness, because the friction factor increased to a maximum and then decreased with increasing Reynolds number. It is therefore possible that the friction factor for the rippled silica deposit could also show this characteristic if the experiments were pursued to a higher Reynolds number. Work is in hand to investigate this further. It is of interest that the friction function Φ, approximately equal to 3 for rippled silica deposit ($\lambda = 7.1$) in the completely rough region as shown on Figure 9, is the same as would be predicted for a rectangular roughness[22] at $\lambda = 7$ if the ratio e/w were taken as 1.5.

5.3 Pressure Drop Effects in Tubes with Simulated Ripple Surfaces

The results of pressure drop measurements taken with the Harwell tubes, and the results of Streeter, are discussed here to see if there is any similarity to the pressure drop characteristics of tubes with naturally-occurring rippled surfaces.

Figures 2(a) and (b) show actual rippled surface profiles, Figure 10 shows profiles of some of the Harwell tubes with the spaced indentations and Figure 6 the profiles of some of Streeter's tubes. The Harwell tubes 17 and 18, which have significant indentations, and are in the series with the smallest x value (2.5 mm), appear as a wavy profile, as also does tube IV of Streeter shown on Figure 6. These

simulated profiles are the nearest in general form to the actual rippled profiles which seem to be wave forms of irregular spacing and slightly smaller radius at the peaks.

The results of Streeter's pressure drop measurements with tubes IV and V demonstrate clearly that the profile shape is most important. Both these tubes have identical dimensions x and e, yet there is a significant difference in the values of their dimensionless friction function Φ as shown on Figure 7. The sharper edges of profile V generate the greater pressure drop. Attempts to construct simulated ripple shapes clearly need to provide fairly detailed similarity of profile in addition to the correct range of values of e, x and λ. Because of the similarity of profile the results of measurements with tube IV can be analysed together with the results of the Harwell tubes.

A plot of the friction function Φ against e^+, as on Figure 12, for the Harwell results obtained with one series of tubes shows that no simple general correlation exists for rippled surfaces, as it does for sand grain roughness, when the only profile dimension considered is the ripple height e (see Eq. (2)). The most obvious other parameter for inclusion in an attempted correlation for Φ is the ripple ratio λ. Unfortunately, such analysis would require Φ vs e^+ plots in the fully rough regime, i.e., where Φ assumes a constant value and is independent of e^+. The initial Harwell experiments only attained this regime for tubes 3, 17 and 18, shown in Figure 12. Taking the results for tube IV of Streeter in conjunction with these three does indicate tentatively that a correlation might be possible. Thus a plot of Φ vs λ shows a curve similar in shape to the curves of Baumann and Rehme[22] for rectangular roughnesses, Figure 5, where a minimum is reached in the region of $\lambda = 7$. However, the range of this plot is too limited at present to permit any firm conclusion, and the possibility is only indicated at this stage. As mentioned in Section 4.2.1, further experiments are required to reach the fully rough regime for others of the simulated ripple surface tubes and generate enough data for a definite correlation.

6. Conclusions

1. Rippled deposit formations can occur in widely different process situations. They are formed in systems operating under isothermal as well as heat transfer conditions, and in pipes covering a large range of diameters, e.g. 1 cm up to 2 m.

2. Ripple deposits show exceptionally high pressure drops compared, for example, to sand-grain-type roughnesses. For identical heights of ripple and sand grain the pressure drop on the rippled surface could be up to 2.5 times that on the sand grain surfaces depending on the Reynolds number.

3. It is postulated that this rippled geometry is formed due to the phenomena of flow separation and reattachment. This only occurs when a system is at, or near, saturation, and where the deposits are strongly adherent.

4. Simulated rippled surfaces have been impressed on a number of 25 mm OD tubes and pressure drops measured in a recent Harwell programme. Analysis of these results in terms of boundary layer theory shows that the roughness height alone is not sufficient to characterise the ripple surface geometry, as is the case for sand-grain-type surfaces. The limited range of data available at the moment tentatively indicates that the ratio of the ripple spacing to the height is the additional parameter required for a general correlation of pressure drop.

Acknowledgements

The authors wish to acknowledge the assistance of Mr. R.K.F. Keeys, Mr. K. Bull and Mr. C.A. O'Keefe with the experimental work and with data processing.

References.

1. Bott, T.R. and Walker, R.A., Chem. Engr. No.255, 391, 1971.

2. Wiederhold, W., Gas-u. Wasserfach, 90, 634, 1949.

3. Seiferth, R. and Kruger, W., VDI-Zeitschrift, 92, 189, 1950.

4. Gessner, W., Chemiker Ztg/Chem. Apparatur, 84, 329, 394, 463, 1960.

5. Schoch, W., Mitt. VGB, 48, 239, 1968.

6. Schoch, W., Richter, R. and Kohle, H., Mitt. VGB, 49, 202, 1969.

7. Schoch, W., Richter, R. and Effertz, P., Maschinenschaden, 43, 65, 1970, CEGB Trans. 5526.

8. Schoch, W., Wiehn, H., Richter, R. and Schuster, H., Mitt. VGB, 50, 277, 1970, CEGB Trans. 5531.

9. Schuster, H., Allianz-Bericht, 16, 28, 1971, CEGB Trans. 5699.

10. Richter, R., Schoch, W., Schuster, H. and Wiehn, H., ASME Paper No.71 - WA/HT - 44,

11. Schoch, W., Wiehn, H., Richter, R. and Schuster, H., Mitt. VGB, 52, 228, 1972.

12. Kohle, H. and Richter, R., Energie, 24, 4, 1972, CEGB Trans. 6090.

13. Haller, K.H., Mravich, N.J. and Seifert, J.W., Mat. Prot. Perf., 10, 27, 1971.

14. Haller, K.H., Lee, R.A. and Slotnik, J.S., ASME Paper No.71 - WA/HT - 45,

15. Foster, G.G. and Garnsey, R., 1971, 'Private Communication'.

16. Garnsey, R., Masterson, H.G. and Tye, R.J., 1971, 'Private Communication'.

17. Heitmann, H.G. and Thomas, D., VGB Speisewassertagung 1966, Risley Trans. 1298.

18. Private Communication, ICI Mond Division.

19. Gudmundsson, J.S. and Bott, T.R., to be published.

20. Coulson, J.M. and Richardson, J.F., "Chemical Engineering", Vol.1, Revised Second Edition, Pergamon Press, 1970.

21. Schlighting, H., "Boundary-Layer Theory", Sixth Edition, McGraw-Hill, 1968.

22. Baumann, W. and Rehme, K., Int. J. Heat Mass Transfer, 18, 1189, 1975.

23. Nikuradse, J., VDI Forsch., 361, 1933, NACA TM-1292.

24. Webb, R.L., Eckert, E.R.G. and Goldstein, R.J., Int. J. Heat Mass Transfer, 14, 601, 1971.

25. Streeter, V.L., Proc. Am. Soc. Civil Eng., 61, 163, 1935.

26. Davies, J.T., "Turbulence Phenomena", Academic Press, 1972.

27. Davies, J.T. and Shawki, A.M., Chem. Engr., No.279, 528, 1973.

28. Lawn, C.J., CEGB Rep. No. RB/B/N3514, 1976.

29. Wilkie, D., Proc. 3rd Int. Heat Transfer Conf., Chicago, 1966.

30. Abbot, D.E. and Kline, S.J., J. Basic Eng., 84, 317, 1962.

31. Lewis, M.J., J. Heat Transfer, 97, 249, 1975.

32. Schlichting, H., Ing.-Arch., 7, 1, 1936.

33. Thomas, R.M., CERL Rep. No. RD/L/N285/72.

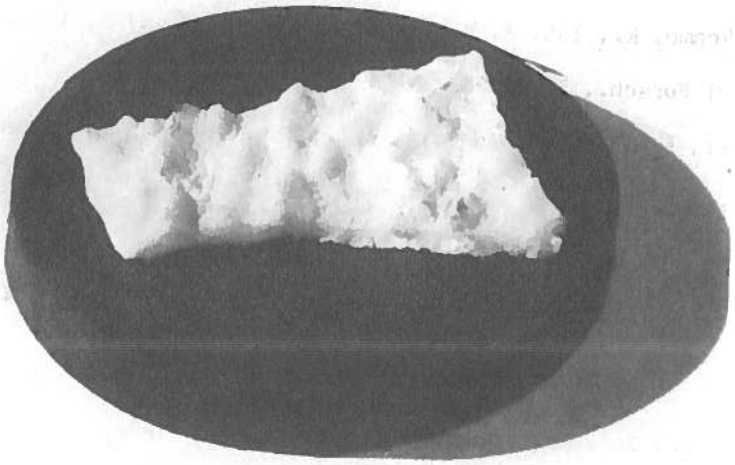

1 cm
0
SCALE

(a) EXAMPLE OF RIPPLED SALT DEPOSITION IN 60 cm. BRINE MAIN.

CONDITIONS :
- SATURATED BRINE SOLUTION FLOW AT APPROX. 15°C.
- REYNOLDS NUMBER 139,000
- DEPOSITION SHOWN AFTER APPROX. 40,000 HRS.
- AVERAGE RIPPLE HEIGHT 1·1 mm.; AVERAGE SPACING 4·7 mm.

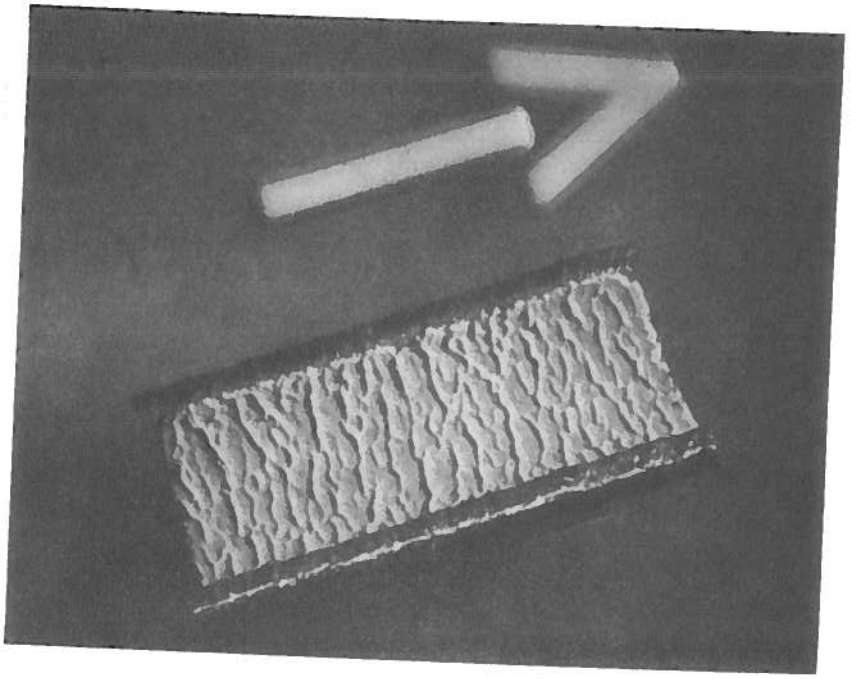

1 cm
0
SCALE

(b) EXAMPLE OF RIPPLED SILICA DEPOSITION.

CONDITIONS :
- GEOTHERMAL WATER FLOW AT APPROX 80°C.
- REYNOLDS NUMBER ≏ 44,000
- DEPOSITION SHOWN AFTER APPROX 2000 HRS.
- AVERAGE RIPPLE HEIGHT = 0·12 mm.; AVERAGE SPACING = 0·87 mm.

FIG. 1. VIEWS OF SOME RIPPLED DEPOSITS.

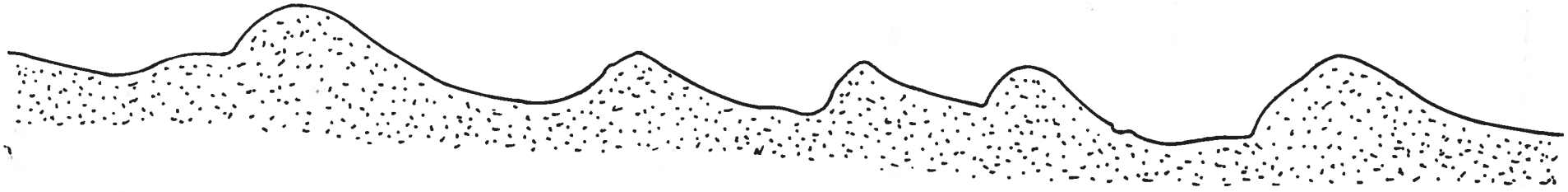

(a) PROFILE OF RIPPLED SURFACE IN BRINE MAIN[18] – MAGNIFICATION x 10

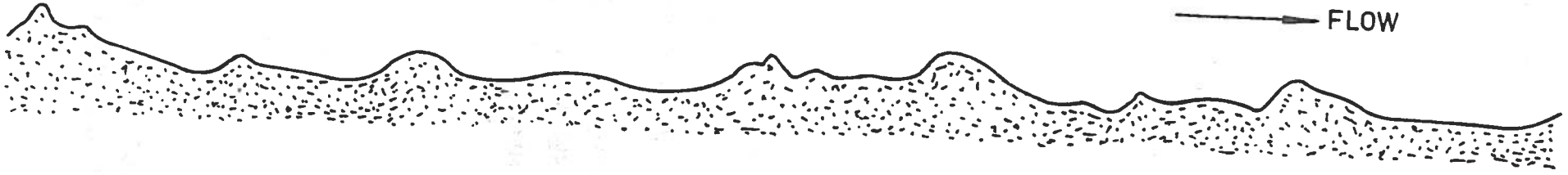

(b) PROFILE OF RIPPLED SILICA SURFACE FROM GEOTHERMAL WATER — MAGNIFICATION x 50.

A.E.R.E. R.8703 FIG. 2. PROFILES OF NATURALLY OCCURING RIPPLED DEPOSITS SHOWN ON FIG 1.

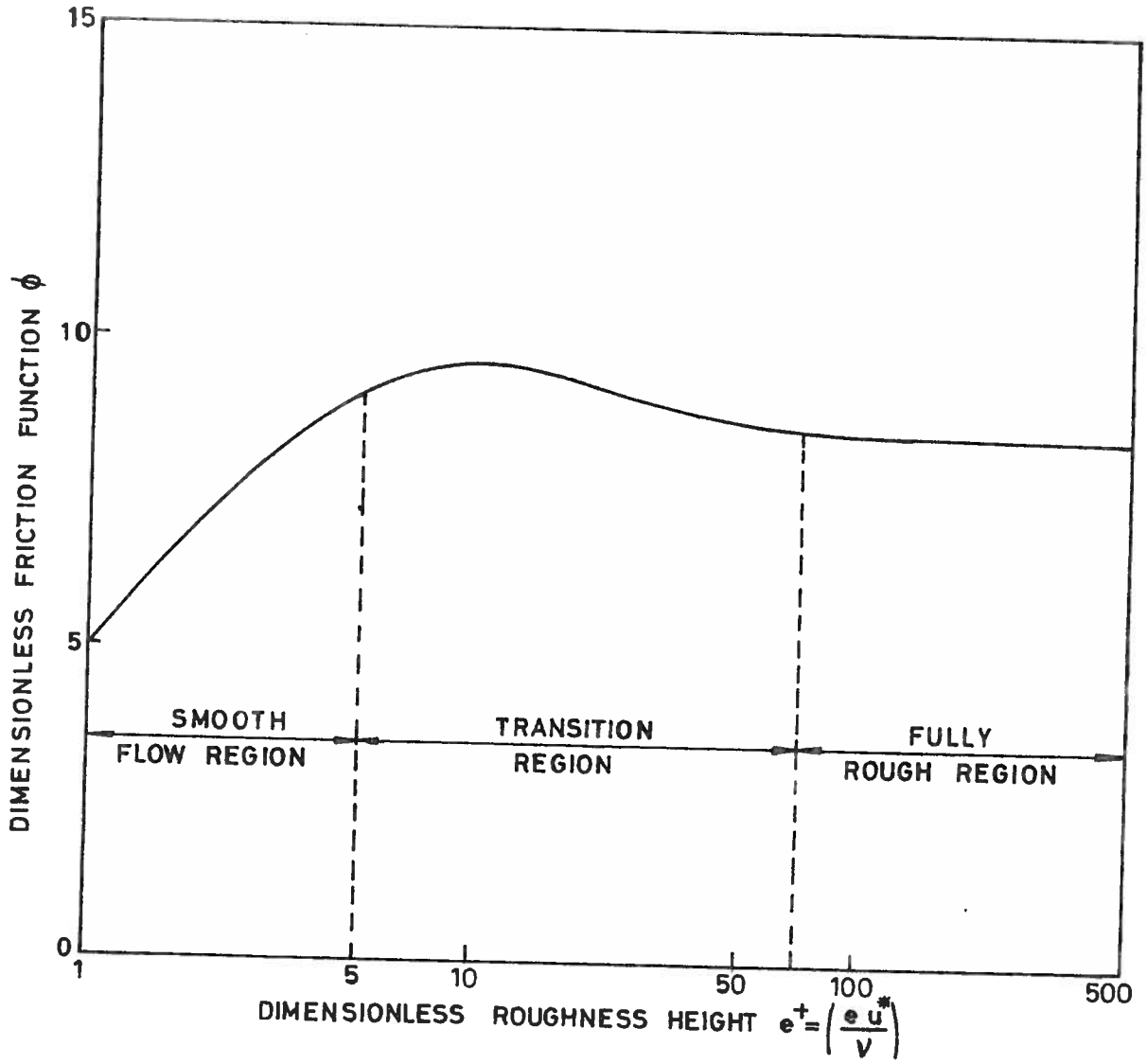

A.E.R.E.R.8703. FIG. 3. CURVE RELATING FRICTION FUNCTION ϕ AND ROUGHNESS HEIGHT e^+ FOR ALL SAND GRAIN SURFACES – BASED ON DATA OF NIKURADSE [21, 23]

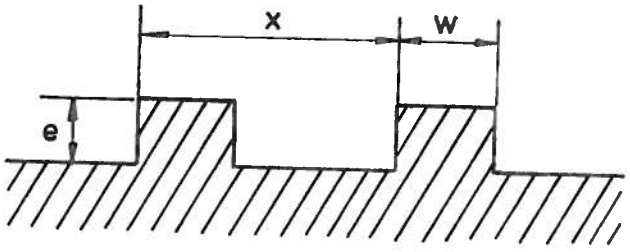

A.E.R.E. R.8703. FIG. 4. GEOMETRY OF RECTANGULAR ROUGHNESSES STUDIED BY BAUMANN AND REHME [22]

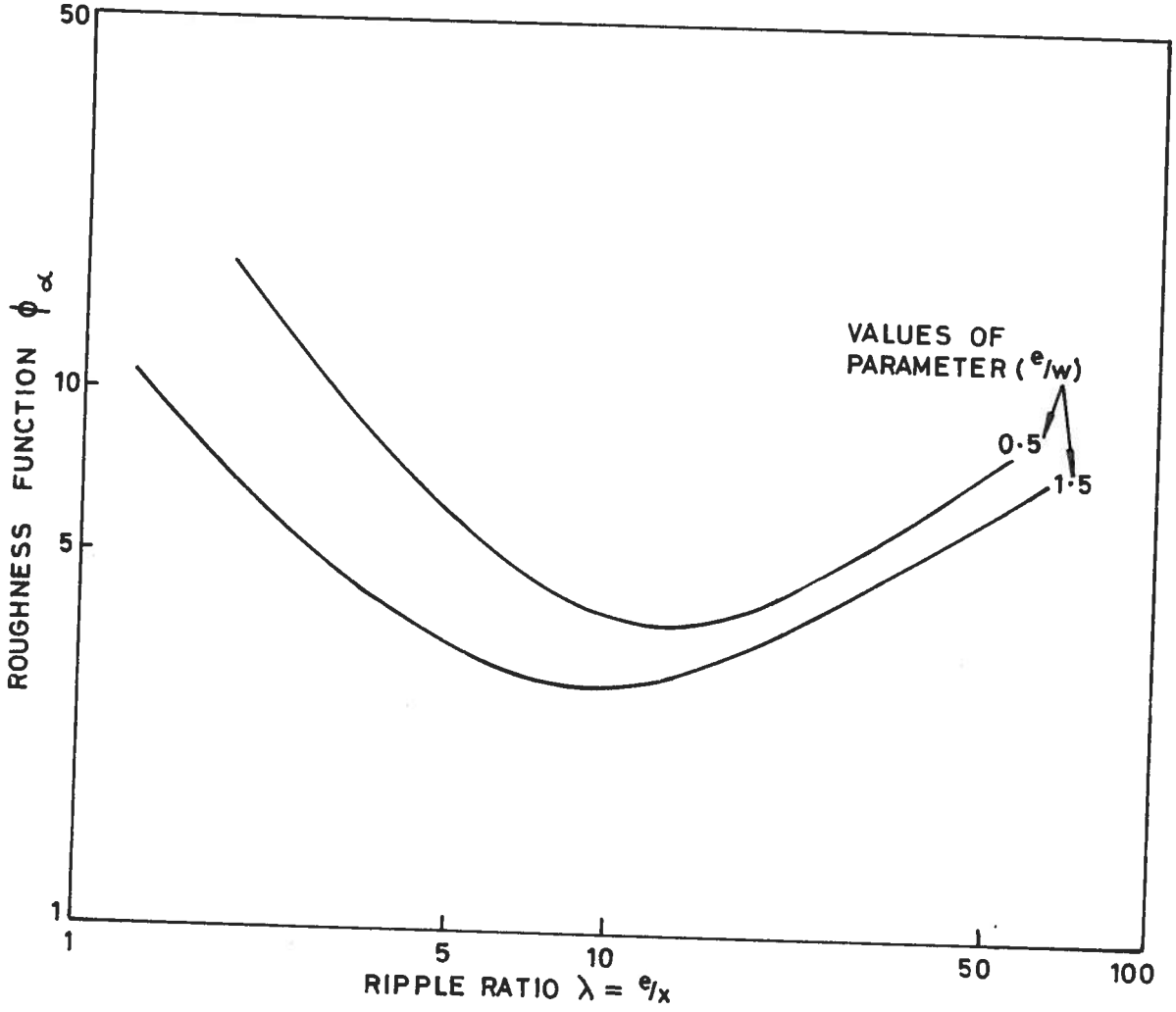

A.E.R.E. R.8703. FIG.5. ROUGHNESS FUNCTION RELATIONSHIP DERIVED BY BAUMANN AND REHME[22] FOR RECTANGULAR ROUGHNESS SHAPES— VALID FOR $e^+ \geqslant 100$.

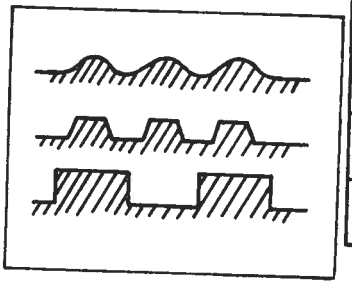

x (mm)	e (mm)	x/e	TUBE NUMBER
0·305	1·10	3·6	IV
0·305	1·10	3·6	V
2·21	0·559	4·0	VII

A.E.R.E. R.8703. FIG.6. PROFILES OF "SCREW THREAD" TYPE ROUGHNESSES INVESTIGATED BY STREETER[25]

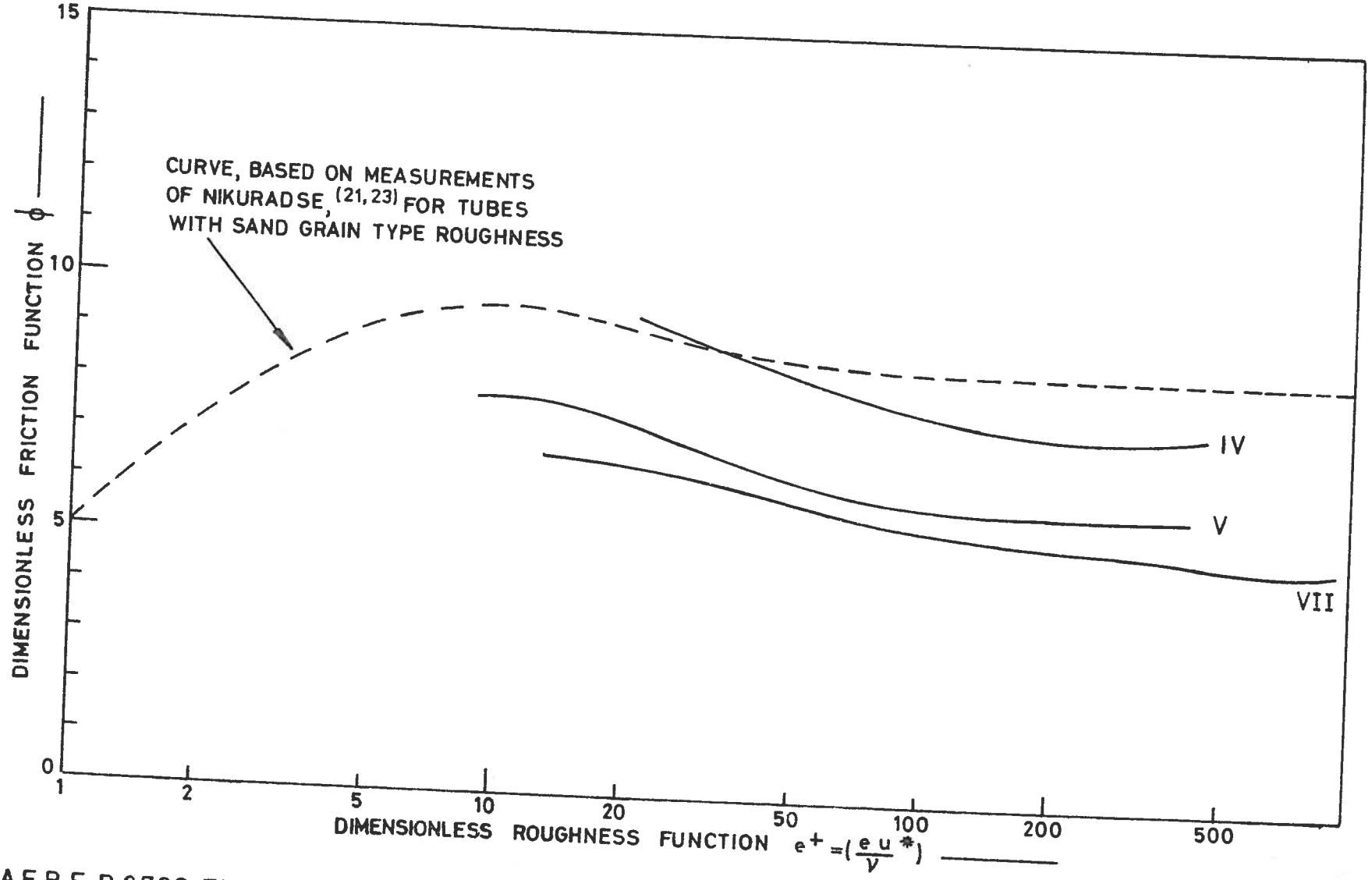

A.E.R.E. R.8703. FIG.7. THE RELATIONSHIP BETWEEN THE DIMENSIONLESS FRICTION AND ROUGHNESS FUNCTIONS FOR TUBES TESTED BY STREETER[25] HAVING SCREW THREAD TYPE ROUGHNESSESS.

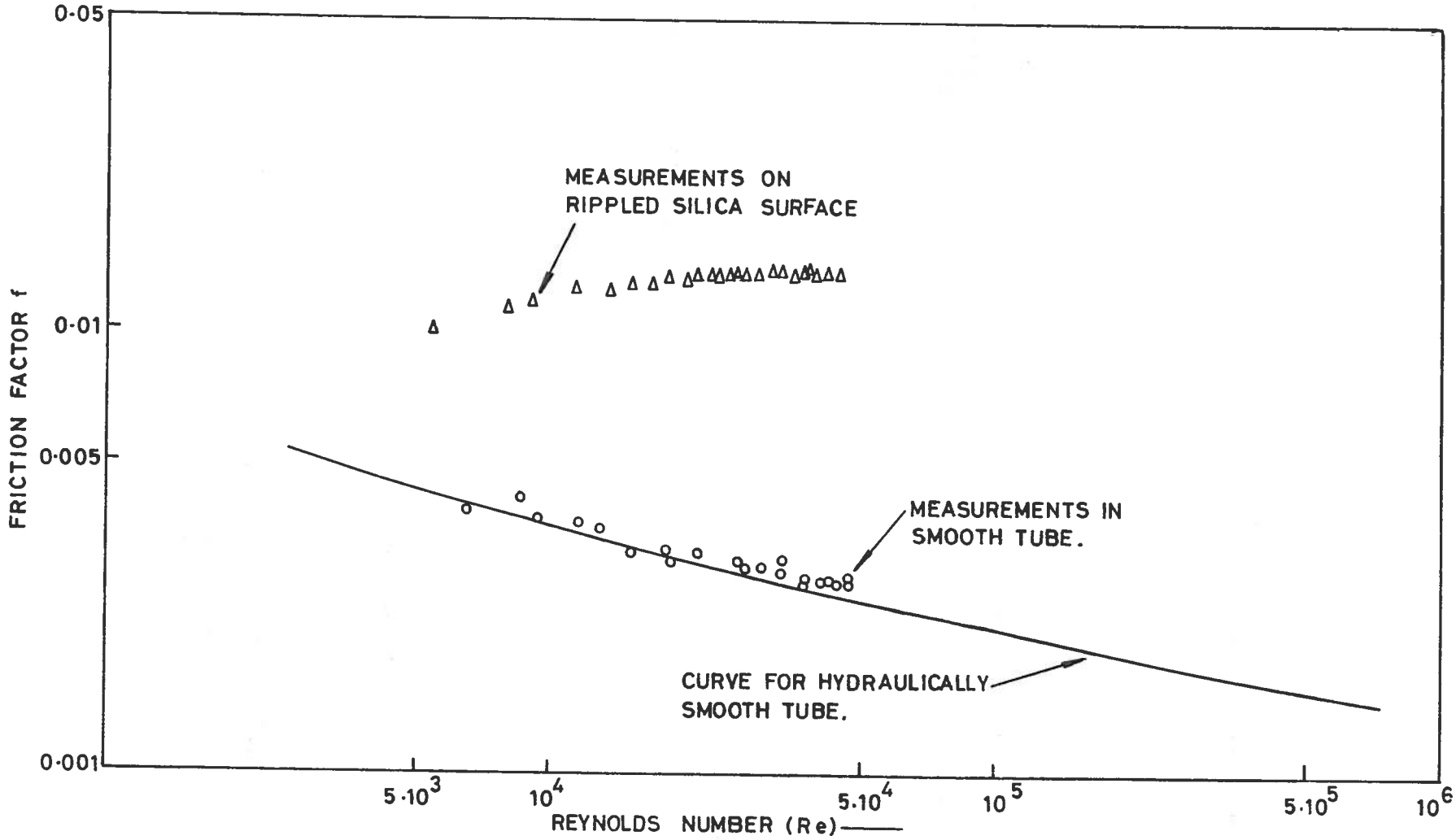

A.E.R.E.R.8703. FIG. 8. FRICTION FACTOR VS REYNOLDS NUMBER FOR SMOOTH TUBE AND TUBE WITH RIPPLED SILICA DEPOSIT

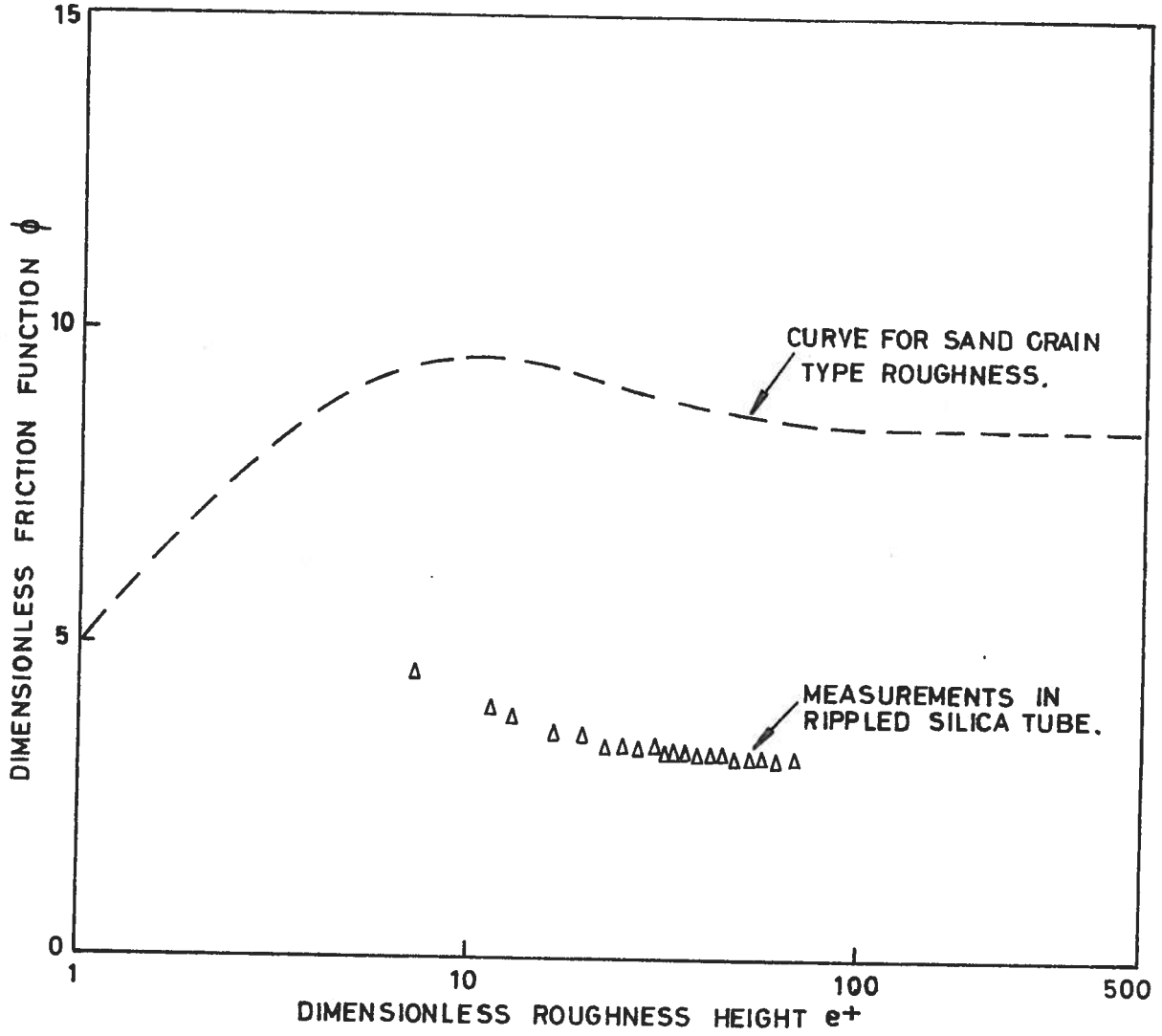

A.E.R.E. R.8703. FIG. 9. FRICTION FUNCTION FOR TUBE WITH RIPPLED SILICA DEPOSIT.

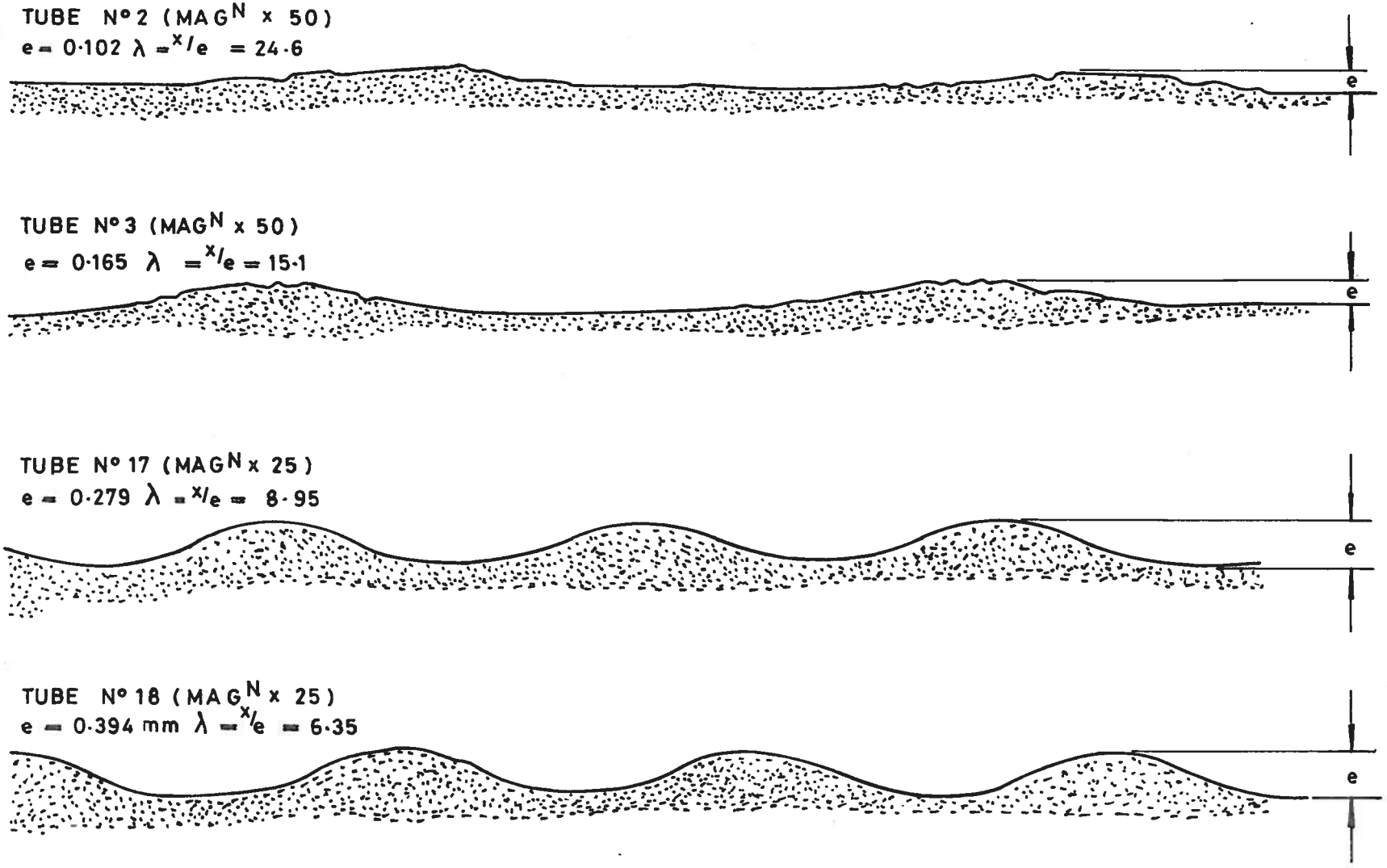

A.E.R.E. R.8703. FIG. 10. PROFILES OF SOME SIMULATED RIPPLED TUBULAR SURFACES MANUFACTURED AT HARWELL. SPACING (X) BETWEEN RIPPLES = 2·5 mm IN EACH CASE.

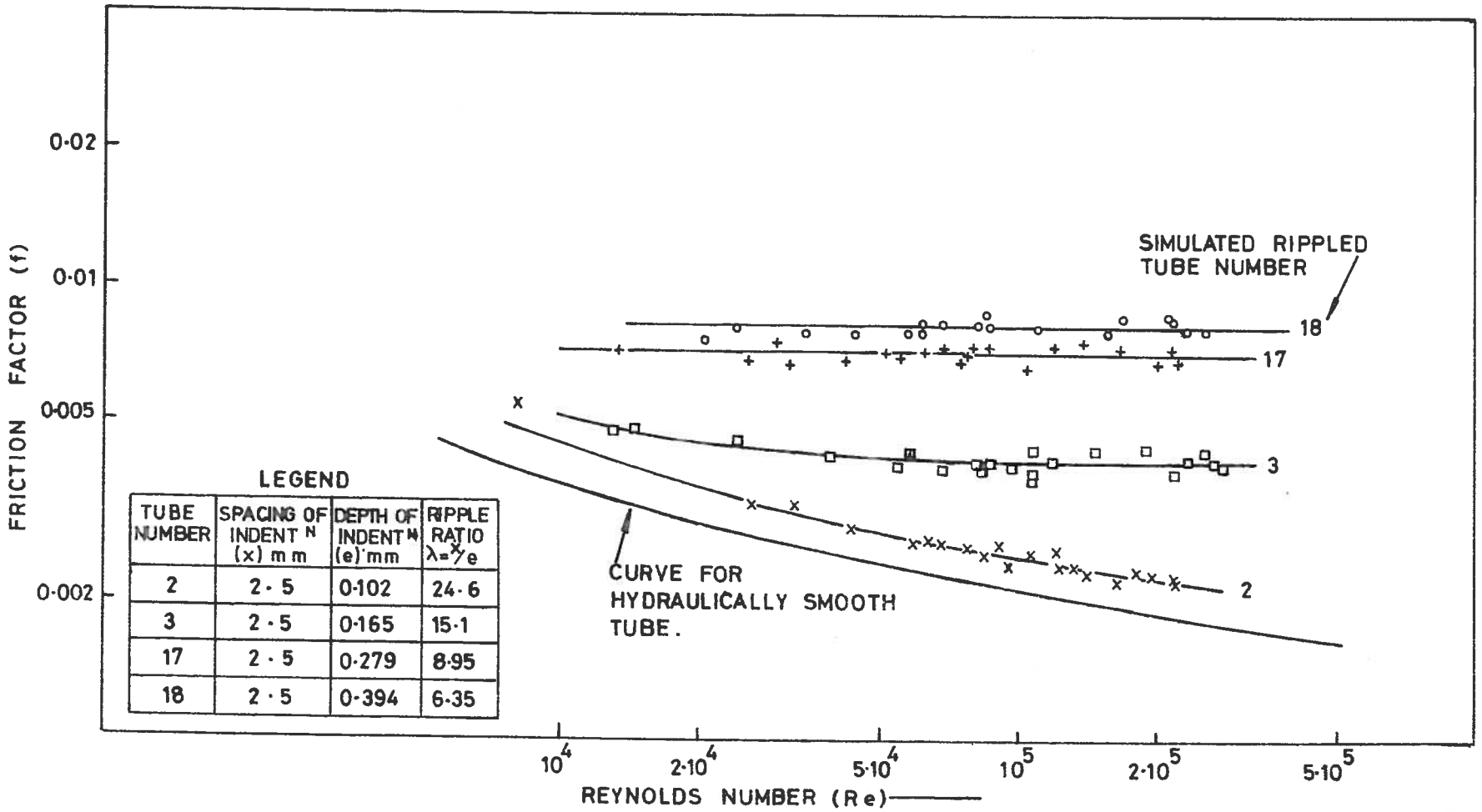

A.E.R.E. R.8703. FIG.11. THE RESULTS OF PRESSURE DROP MEASUREMENTS ON SOME TUBES WITH SIMULATED RIPPLE SURFACES.

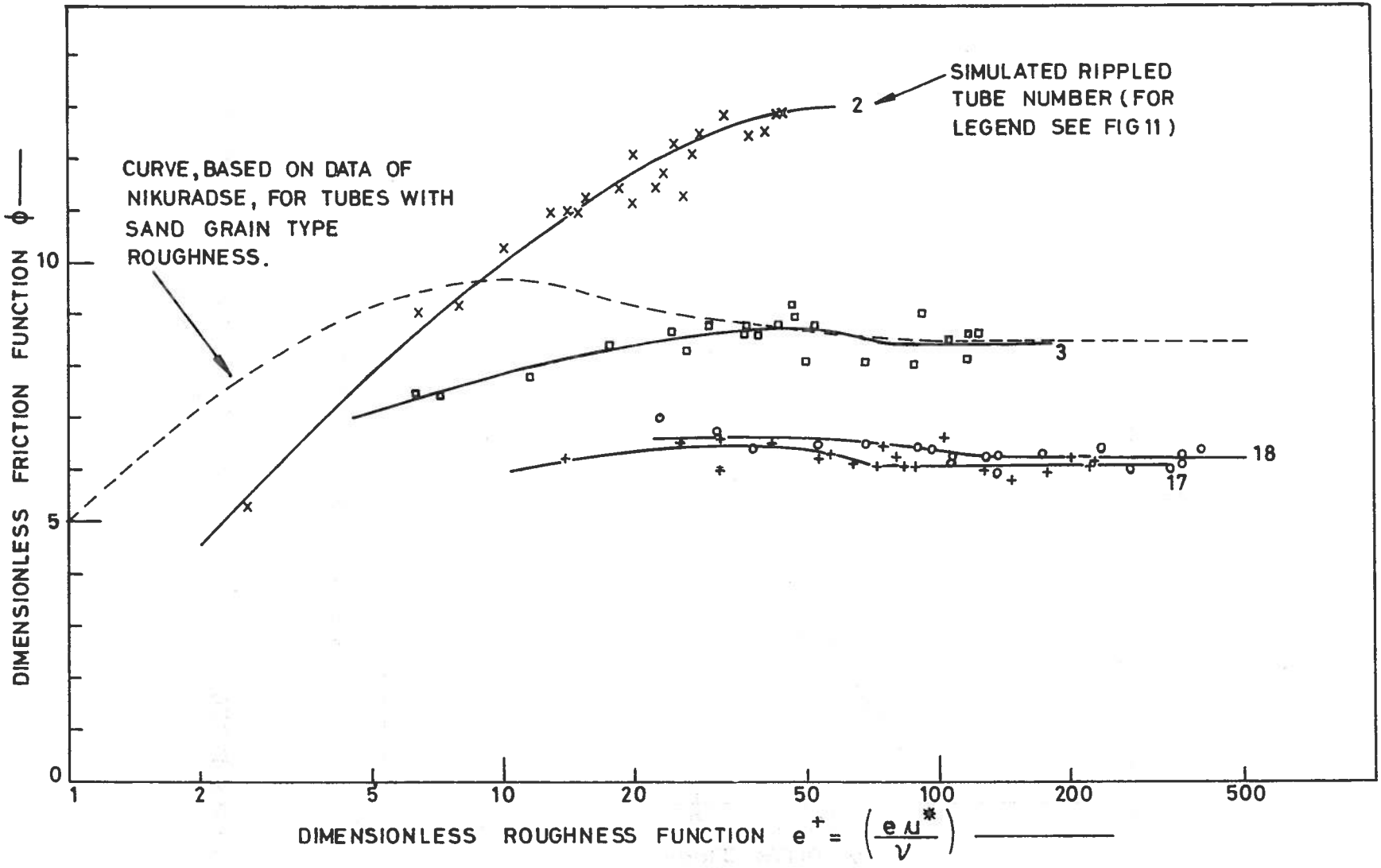

A.E.R.E.R.8703. FIG.12. THE RELATIONSHIP BETWEEN THE DIMENSIONLESS FRICTION AND ROUGHNESS FUNCTIONS FOR SOME TUBES WITH SIMULATED RIPPLED SURFACES.

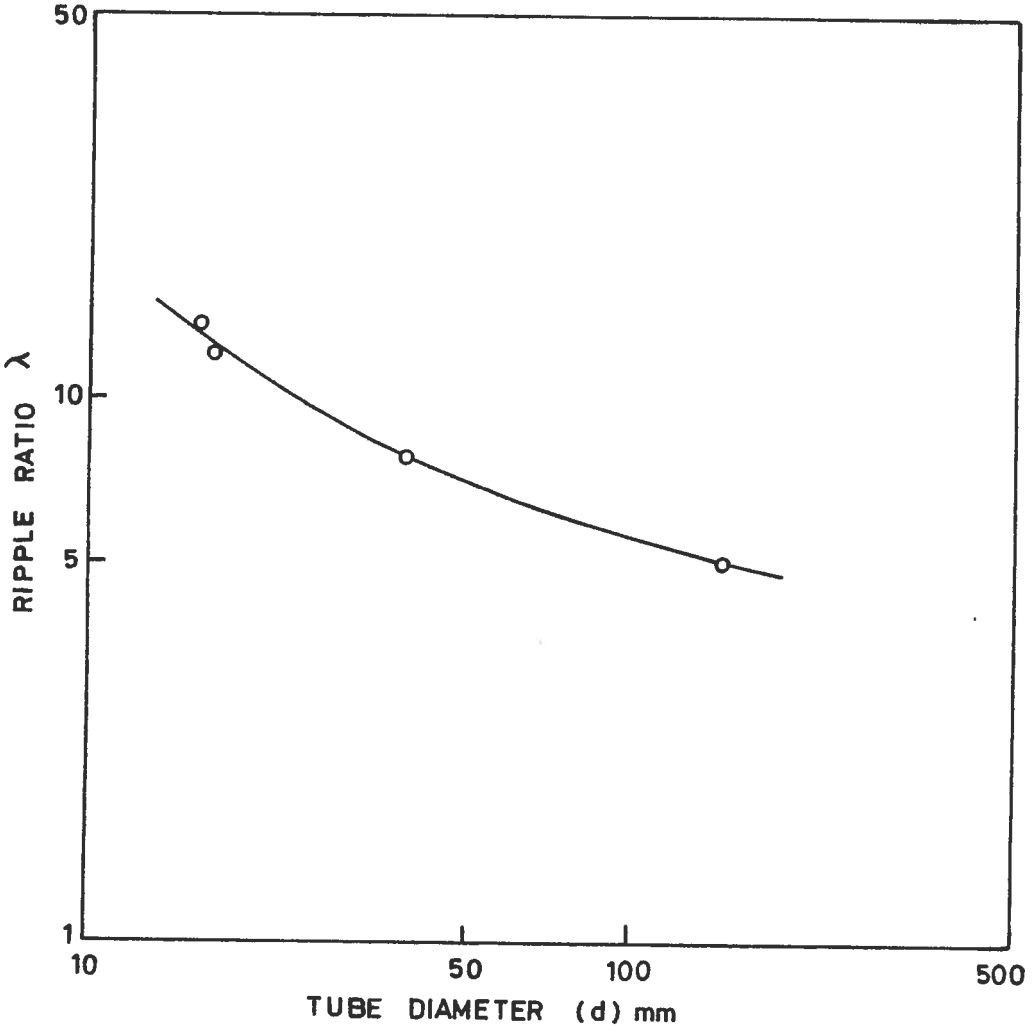

A.E.R.E. R.8703. FIG.13. ACTUAL RIPPLE RATIO VS TUBE DIAMETER FOR BOILER TUBES.

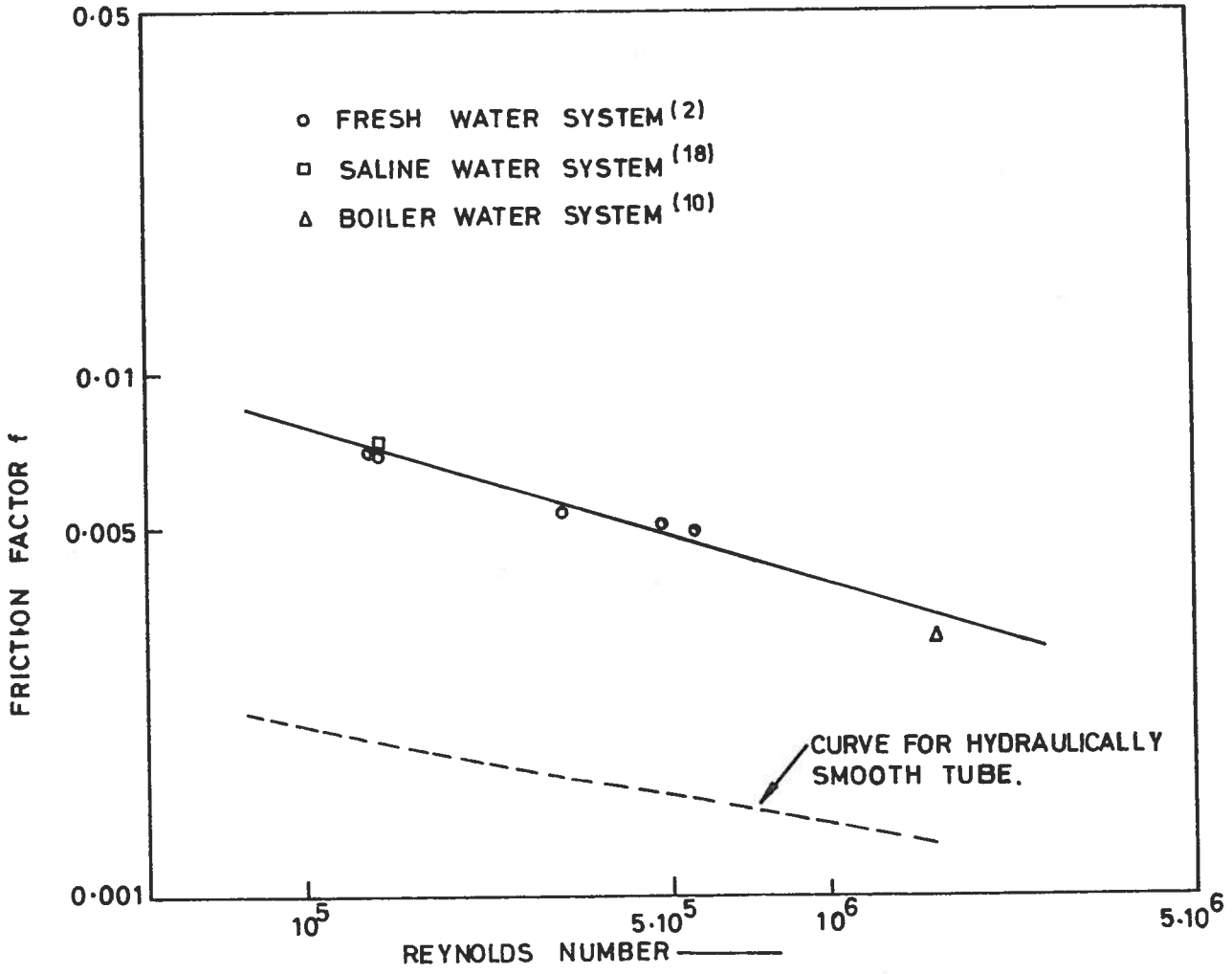

A.E.R.E. R.8703. FIG.14. FRICTION FACTOR VS REYNOLDS NUMBER FOR PIPES WITH RIPPLED SURFACES IN THREE DIFFERENT SYSTEMS.